LRP 473/93 April 1993

STUDIES OF SELF-CONSISTENT FIELD STRUCTURE IN A QUASI-OPTICAL GYROTRON

T.M. Antonsen Jr., A. Bondeson, M. Roulin, and M.Q. Tran

submitted for publication in

Physics of Fluids B

STUDIES OF SELF-CONSISTENT FIELD STRUCTURE IN A QUASI-OPTICAL GYROTRON

T.M. Antonsen Jr.*, A. Bondeson, M. Roulin, and M.Q. Tran

Centre de Recherches en Physique des Plasmas
Association Euratom - Confédération Suisse
Ecole Polytechnique Fédérale de Lausanne
21, Ave des Bains, CH-1007 Lausanne - Switzerland

* Laboratory for Plasma Research, Univ. of Maryland at College Park, College Park, MD 20742, U.S.A.

ABSTRACT - The presence of an electron beam in a quasi-optical gyrotron cavity alters the structure of the fields from that of the empty cavity. A computer code has been written which calculates this alteration for either an electron beam or a thin dielectric tube placed in the cavity. Experiments measuring the quality factor of such a cavity were performed for the case of a dielectric tube and the results agree with the predictions of the code. Simulations of the case of an electron beam indicate that self-consistent effects can be made small in that almost all the power leaves the cavity in a symmetric gaussian-like mode provided the resonator parameters are chosen carefully.

I. INTRODUCTION

The need for high average power sources of coherent millimeter wave radiation has lead to the conception[1] of the quasi-optical gyrotron.[2-4] The quasi-optical gyrotron differs from conventional gyromonotrons[5] in that the interaction between the radiation and the injected electron beam takes place in an open, optical resonator as opposed to a cylindrical, tube shaped cavity. The purpose of the open resonator is two fold. First, the resonator, which is defined by two circular, spherical mirrors, can be made quite large, thereby lowering the peak power dissipation in the mirrors relative to that in a corresponding gyromonotron. Second, the use of an open resonator effectively eliminates many modes which might otherwise compete with the operating mode. While advances have been made in the design of conventional cavity gyrotrons[6-8] which minimize or eliminate mode competition, the problem of power dissipation in the walls of these gyrotron cavities is still severe. Thus, the advantage of the quasi-optical gyrotron in controlling the peak power dissipation in the cavity is of importance.

All previous analyses[1,2] of the operation of quasi-optical gyrotrons have made the assumption that the radiation field is dominantly a superposition of eigenmodes of the empty cavity with perhaps a small additional electrostatic component.[9,10] Equivalently, it is assumed that the power extracted from the electron beam is converted to radiation in eigenmodes of the cavity. Due to the open nature of the cavity, it is reasonable to ask whether power from the beam can be converted to radiation which escapes directly from the cavity.

A simple estimate can be given showing that this effect will become important if one attempts to design a sufficiently low Q cavity. Consider the beam to be a localized current distribution oscillating at frequency ω,

$$\mathbf{j} = \frac{1}{2}\,\mathbf{e}_x\,(j_x(x)\,e^{-i\omega t} + c.c.) \qquad (1)$$

Here we have taken the current density, $\mathbf{j}$, to point in the x direction of a cartesian coordinate system in which the axis of the cavity is aligned parallel with the y axis, and the magnetic field is aligned parallel with the z axis. Neglecting for the moment the effect of the cavity mirrors one can calculate the angular distribution and the amount of power radiated by the beam[11],

$$P_R = \int d\Omega \frac{dP_R}{d\Omega} = \frac{k^2}{8\pi c} \int d\Omega\,(1-n_x^2) \left| \int d^3x\, j_x\, e^{-ikn\cdot x} \right|^2 \qquad (2)$$

where the integral is over the solid angle defined by the unit vector $\mathbf{n}$, giving the direction of the radiated power, $k = \omega/c$ is the wave number of the radiation, and c is the speed of light. Thus, the power radiated is proportional to the square of the current, and its angular distribution depends on the spatial distribution of the current density. A similar expression can be obtained if one supposes instead that all the power is radiated into a single mode of the cavity which in the vicinity of the electron beam has the spatial form,

$$\mathbf{E} = \frac{1}{4}\,\mathbf{e}_x\,(u_+(\mathbf{x})\,e^{iky} + u_-(\mathbf{x})\,e^{-iky})\,e^{-i\omega t} + c.c.\,, \qquad (3)$$

representing two counter propagating waves with slowly varying envelopes $u_\pm$. The expression for the radiated power is again proportional to the square of the current, but also depends on the total power output coupling T of the two mirrors (the combined power transmission coefficient of the two mirrors) which define the cavity,

$$P_c = \frac{\pi \left| \int d^3x (u_+(\mathbf{x})\, e^{iky} + u_-(\mathbf{x})\, e^{-iky})\, j_x^* + c.c. \right|^2}{2cT \int dxdz\, |u_+|^2} . \qquad (4)$$

Here, we have assumed that the current is oscillating at a frequency which corresponds exactly to that of the cavity mode in question.

In reality, the radiated field will be a mixture of both the free space radiation implied by (2) and the cavity field (3). An estimate of the importance of the free space radiation can be made by taking the ratio of (2) to (4) for an assumed current distribution. To make this estimate we assume the current distribution corresponds to that of a pencil beam, with a gaussian distribution along the z direction (the direction of the applied magnetic field) with a width equal to the spot size of the cavity radiation field,

$$j_x = i_0 \exp(-z^2/r_0^2)\, \delta(x)\delta(y).$$

Upon performing the integrations one obtains,

$$P_R/P_c = \frac{\pi^{3/2}}{16\sqrt{2}} T \frac{r_0}{\lambda} \cong 0.25T\frac{r_0}{\lambda}, \qquad (5)$$

where λ is the wavelength of the radiation and we have assumed the spot size r_0 is much greater than the wavelength λ. For typical parameters the transmission T is 0.1, and the ratio of the spot size to the wavelength is 4. Thus, free space radiated power is a non negligible amount. This amount will increase as one goes to smaller wavelength and larger output coupling.

The angular distribution of the free radiation power is such that it will be difficult to collect in a controlled manner. In particular, for the pencil beam, it follows from (2) that the power is directed in an asymmetrical cone. The cone is narrow in the z direction because the current distribution

is extended along this direction (the direction of the applied magnetic field). The cone is very wide in the x direction because the pencil current distribution is localized in the x direction. Most gyrotron beams are not pencil beams, but rather, are annular beams, with a radius of the order of the wavelength of the radiation. Larger size beams will radiate into a smaller cone reducing the ratio (5). However, for beams with size of the order of a wavelength the cone will still be rather broad.

The purpose of this paper is to present a study of the modifications of the fields of an open resonator by a distribution of currents such as would be expected in a quasi-optical gyrotron. Section 2 of this paper presents a mathematical formulation of the problem which is suitable for numerical solution. Section 3 presents solutions obtained in the case in which the current distribution is induced in a dielectric tube placed across the axis of the cavity. In this case the presence of the tube alters the frequency and damping rate of the modes of the cavity. The results of the calculation are then compared with those of an experiment thereby testing the validity of the calculation. Section 4 presents the results of calculations in which the distribution of currents is determined self consistently for a gyrating electron beam. It is found that for the parameters of present day experiments, nearly all of the radiated power is intercepted by the mirrors. Thus, the problem of free space radiation is not likely to be the cause of the observed, poorer than expected, efficiency in quasi-optical gyrotrons.

II. MATHEMATICAL FORMULATION

A. Paraxial approximation

To study the perturbation of the fields by a small object (such as an electron beam or a dielectric rod) in an open, quasi-optical resonator we

will assume that the paraxial approximation is valid. That is, we assume that the radiation consists dominantly of two counter propagating beams aligned with the axis of the cavity. This requires, in principle, that the scattering object be sufficiently large and sufficiently transparent so that radiation suffers only small angle scattering as it passes over the object. In terms of the expression for the free power radiated (2) we require that the current distribution be sufficiently smooth in the x-z plane so that the power is radiated into a narrow cone directed along the y axis. This condition is only marginally satisfied in the experiments and we will have to introduce some ad hoc procedures to account for the large angle radiation. The present method will be suitable for analyzing a high Q cavity in which the amount of radiation which misses the mirrors due to scattering by the object is a small fraction of the radiation incident on the mirrors. This scattered radiation may still represent a large amount of power, which can be comparable to that which is intentionally coupled out of the cavity, either by spillover, or by partially transmitting mirrors. Thus, the calculation will apply to cases where the hot Q of the cavity is changed by a factor of order unity from the cold Q value.

We now describe the geometry under consideration. The cavity is defined by two spherical mirrors with its axis chosen to coincide with the y axis of a Cartesian coordinate system. The dielectric rod, or electron beam, is chosen to lie along the z axis in the vicinity of x and y = 0. We consider the radiation to be plane polarized with its electric field dominantly in the x direction. This polarization is the one that interacts most strongly with a gyrating electron beam. The radiation will be affected by the currents in the scatterer which are also directed along the x axis. We assume that all fields and currents are oscillating at a single frequency, ω, and write,

$$\mathbf{E} = \frac{1}{2}\,\mathbf{e}_x\,(E_x\,e^{-i\omega t} + \text{c.c.})\,, \tag{6a}$$

$$\mathbf{J} = \frac{1}{2}\,\mathbf{e}_x\,(J_x\,e^{-i\omega t} + c.c.)\ . \qquad (6b)$$

We then write the scalar wave equation relating the components of the current density and radiation electric field,

$$\nabla^2 E_x + k^2\,E_x = -\,ik\,\frac{4\pi}{c}\,J_x \qquad (7)$$

where $k = \omega/c$. Equation 7 is only valid if the radiation wave vector is dominantly perpendicular to x. Otherwise, it is necessary to include other components of the current density and electric field. We, however, will assume that the radiation wave vector is aligned dominantly along the axis of the cavity, and we will decompose the electric field into waves propagating in both directions along the y axis,

$$E_x(\mathbf{x}) = \frac{1}{2}\left(E_+(\mathbf{x})\,e^{iky} + E_-(\mathbf{x})\,e^{-iky}\right). \qquad (8)$$

The amplitudes of the forward and backward propagating waves then satisfy the paraxial equation,

$$\left(\nabla_\perp^2 \pm 2ik\frac{\partial}{\partial y}\right) E_\pm = -\,2ik\,\frac{4\pi}{c}\,J_x\,\exp(\pm iky)\ , \qquad (9)$$

where

$$\nabla_\perp^2 = \frac{\partial^2}{\partial x^2} + \frac{\partial^2}{\partial z^2}$$

is the Laplacian transverse to the axis of the cavity.

The system of equations for the field is completed by expressing the boundary conditions on the surfaces of the two mirrors. The locations of the surfaces of the two mirrors are given by

$$y = d_r - \frac{1}{2} x_\perp^2 / R_{cr}$$

$$y = - (d_l - \frac{1}{2} x_\perp^2 / R_{cl})$$

for the right and left mirror respectively. Here $\mathbf{x}_\perp = (x,z)$ gives the location of a point relative to the y axis, and R_{cl} and R_{cr} are the radii of curvature of the mirrors. We assume that the surfaces of the mirrors are not perfectly conducting, but rather, they are partially reflecting and are characterized by reflection coefficients ρ_r and ρ_l. Here ρ_r and ρ_l are defined such that for perfectly conducting mirrors $\rho_r = \rho_l = 1$. As a result, the amplitudes of the forward and backward propagating waves are related by

$$E_-(\mathbf{x}_\perp, d_r) = - \rho_r \exp\left(2ik \frac{d_r - \frac{1}{2} x_\perp^2}{R_{cr}} \right) E_+ (\mathbf{x}_\perp, d_r) \qquad (10a)$$

and

$$E_+(\mathbf{x}_\perp, d_l) = - \rho_l \exp\left(2ik \frac{d_l - \frac{1}{2} x_\perp^2}{R_{cl}} \right) E_- (\mathbf{x}_\perp, d_l) \, . \qquad (10b)$$

Note, that consistent with the paraxial description of the fields, we may take the mirror surfaces to be located at d_r and $-d_l$ when evaluating the amplitudes of the wave fields, but must include the deviations from these values due to the curvature of the mirrors in evaluating the rapidly varying exponential factors. The above relations hold for $\mathbf{x}_\perp$ values on the surfaces of the mirrors only. That is, for

$$x_\perp^2 \le R_{mr} \quad \text{and} \quad x_\perp^2 < R_{ml}$$

where R_{mr} and R_{ml} are the radii of the right and left mirrors.

To solve the field equations we assume, for the moment, that the current distribution on the scatterer is known. Then, the amplitude of the forward propagating wave on the right mirror can be expressed as the sum of contributions from the scatterer and the amplitude of the forward propagating field on the left mirror.

$$E_+ (\mathbf{x}_\perp, d_r) = \int_{Lm} d^2 x'_\perp \, K(\mathbf{x}_\perp, \mathbf{x}'_\perp, \sigma_t) \, E_+(\mathbf{x}'_\perp, -d_l) - \int d^3x' \, K(\mathbf{x}_\perp, \mathbf{x}'_\perp, \sigma'_r) \, \frac{4\pi}{c} J_x (\mathbf{x}') \, e^{-iky'} \tag{11}$$

where the Green's function kernel satisfying the paraxial equation is given by

$$K(\mathbf{x}_\perp, \mathbf{x}'_\perp, \sigma) = \frac{1}{2\pi\sigma} \exp\left(- \frac{(\mathbf{x}_\perp - \mathbf{x}'_\perp)^2}{2\sigma} \right) \tag{12}$$

and σ_t and σ'_r are given in terms of the distance between the two mirrors and the distance along the axis from a point on the scatterer to the right mirror,

$$\sigma_t = \frac{i(d_r + d_l)}{k} \tag{13a}$$

$$\sigma'_r = \frac{i(d_r - y')}{k} \tag{13b}$$

A similar expression can be written from the backward propagating wave,

$$E_- (\mathbf{x}_\perp, -d_l) = \int_{Rm} d^2 x'_\perp \, K(\mathbf{x}_\perp, \mathbf{x}'_\perp, \sigma_t) \, E_-(x'_\perp, d_r) - \int d^3x' \, K(\mathbf{x}_\perp, \mathbf{x}'_\perp, \sigma'_l) \, \frac{4\pi}{c} J_x (x') \, e^{iky'} \, . \tag{14}$$

where σ_l' is given by,

$$\sigma_l' = \frac{i(d_l + y')}{k} \quad . \tag{15}$$

We will now make the additional approximation that the size of the scatterer is small compared with the distance to either of the mirrors,

$$\sigma_r' \cong \sigma_r = \frac{idr}{k} \qquad \sigma_l' \cong \sigma_l = \frac{id_l}{k} .$$

An equivalent approximation is to disregard the transverse Laplacian in Eq. (9) while calculating the field in the vicinity of the scatterer. Thus, we can calculate from (9) the change in amplitude of the forward and backward propagating waves upon traversing the region of the scatterer,

$$\Delta E_{\pm}(\mathbf{x}_\perp) = - \int_{-\infty}^{\infty} dy' \frac{4\pi}{c} J_x(\mathbf{x}_\perp, y') \, e^{\pm iky'} \, . \tag{16}$$

In terms of this change in amplitude, $\Delta E_+(\mathbf{x})$, the field on opposing mirrors expressed in Eq. (11) is rewritten,

$$\begin{aligned} E_+(\mathbf{x}_\perp, d_r) = & \int_{Lm} d^2x_\perp' \, K(\mathbf{x}_\perp, \mathbf{x}_\perp', \sigma_t) \, E_+(\mathbf{x}_\perp', -d_l) \\ & + \int d^2x_\perp' \, K(\mathbf{x}_\perp, \mathbf{x}_\perp', \sigma_r) \, \Delta E_+(\mathbf{x}_\perp') \end{aligned} \tag{17}$$

with a similar equation applying to $\Delta E_-(\mathbf{x})$.

B. Self-field

Equation (17) and its counterpart for the backward propagating wave are sufficient for calculating the field pattern on the mirrors, far from the

beam. However, to self-consistently determine the beam current we must have an expression for the electric field at the beam which includes the self-field induced by the beam current.

The indefinite versions of Eq. (16) can be used to find the self-field at the beam for sufficiently smooth current distributions. If we represent the amplitude of the incident forward propagating wave at the scatterer as $E_+(\mathbf{x}_\perp,-0)$, then the field at a point in the scatterer can be written,

$$E_+(\mathbf{x}_\perp,y) = E_+(\mathbf{x}_\perp,-0) \pm \int_{-\infty}^{y} dy' \frac{4\pi}{c} J_x(\mathbf{x}_\perp,y')\, e^{-iky'} . \qquad (18)$$

This expression is well behaved for smooth current distributions. It is not well behaved if one assumes, as we would like, that the current is distributed on an infinitely thin annulus. In this case, the self-field term in the above exhibits a square root singularity as x approaches the radius of the annulus. As a result, quantities such as the electric field energy density and the ohmic power density, $\mathbf{j} \cdot \mathbf{E}$, diverge. However, no such divergence occurs in the expression for the electric field on the opposing mirrors, that is Eq. (17) is still valid. The discrepancy is related to the fact that the paraxial approximation assumes that the radiated power is emitted in a narrow cone around the axis of the cavity. A singular current distribution, such as that of an annulus, radiates power in a large cone, whose angular width goes to infinity in the paraxial approximation. As a result, if we were to calculate all the power passing through the plane of the mirror, $y = d_r$, it too would diverge for a singular current.

The physical resolution of the problem is that the power is restricted to a cone with a maximum angle of 90 degrees. Such a restriction has a negligible effect on the fields calculated on the mirrors, but it requires a modification of the way in which the self-field is calculated at the beam. One way to eliminate the divergence at unphysical angles is to smooth the

current distribution over a distance of a wavelength, before the scattered radiation is calculated. Smoothing over a wavelength eliminates radiation that, in the paraxial approximation, is radiated into unphysical angles.

To determine an appropriate form of the smoothing function, we return to the expression for the power radiated into free space Eq. (2) by a current distribution such as the one considered here. Since the power radiated must equal the volume integral of $\mathbf{J} \cdot \mathbf{E}$ we can define a component of the local electric field amplitude

$$\mathbf{E}_s = \frac{1}{2} \mathbf{e}_x \left(E_{sx} \exp(-i\omega t) + E_{sx}^* \exp(i\omega t) \right)$$

which is associated with the far field radiation,

$$E_{sx} = \frac{-k^2}{4\pi c} \int d\Omega \, (1 - (\mathbf{n} \cdot \mathbf{e}_x)^2) \int d^3x' \, J_x \, e^{-ik\mathbf{n}\cdot(\mathbf{x}'-\mathbf{x})} . \qquad (19)$$

This definition leads by construction to the power balance relation

$$P_R = - \int d^3x \, \langle \mathbf{J} \cdot \mathbf{E}_s \rangle = - \frac{1}{4} \int d^3x \, (J_x E_{sx}^* + \text{c.c.}) , \qquad (20)$$

where P_R is the power radiated by the current distribution, Eq. (2). The actual self-field of the beam consists of a superposition of the field given by Eq. (19) and reactive components which lead to no net power radiation. For example, a portion of the field is electrostatic. While this field does not contribute directly to the power extracted from the beam it has an indirect effect on the power extracted from the beam, since it modifies the electron trajectories and consequently the current density. We will not include this effect here so that we may focus attention on the power radiated direction into different angles in the far field. The effect of the electrostatic self-field on quasi-optical gyrotron operation has been studied previously.[7,8]

We first change variables in the angular integration in Eq. (19) from the solid angle Ω to the two components n_x and n_z of the unit vector $\mathbf{n}$,

$$E_{sx} = -\frac{k^2}{4\pi c}\int d^3x'\, J_x(\mathbf{x}')\sum_{n_y}\int\frac{dn_x dn_z}{|n_y|}(1-n_x^2)\times \exp\Big(ik\big(n_x(x'-x)+n_y(y'-y)+n_z(z'-z)\big)\Big) \tag{21}$$

where $n_y = \pm\sqrt{1-n_x^2-n_z^2}$ and the integral over n_x and n_z corresponds to $n_y^2 > 0$. The paraxial result, Eq. (18), is obtained by assuming that the dependence of J_x and x' and z' is smooth on the scale of a wavelength such that the Fourier transform of J_x is concentrated at small values of n_x and n_z. The following approximations are then made in the integrand in Eq. (21): $(1 - n_x^2) \cong 1$; $n_y \cong \pm 1$ (small scattering angles) and the range of integration for n_x, n_z is allowed to run from $-\infty$ to ∞.

The result is

$$E_{sx} = \frac{1}{2}\left(E_{s+}\, e^{iky} + E_{s-}\, e^{-iky}\right)$$

where

$$E_{s\pm}(x,y,z) = -\frac{1}{2}\frac{4\pi}{c}\int_{-\infty}^{\infty} dy'\, J_x(x,y',z)\, e^{\pm iky'} \tag{22}$$

which differs from Eq. (18) only by the presence of a reactive field. That is, the expressions for the self-fields given by (18) and (22) lead to the same radiated power.

As mentioned, the problem with the above procedure is that for non smooth current distributions their Fourier transforms are not negligibly small for all values of n_x and the behavior of integrand for $n_x \cong 1$ must be treated.

A modified evaluation of Eq. (21), which we will use here, proceeds as follows. We again assume the Fourier transform of the current distribution is

peaked at small values of n_z owing to the smoothness of the current in the direction of the applied magnetic field, but we allow n_x to be arbitrary. Further, we replace n_y by ± 1 in the exponent in Eq. (21). (This allows for a separation of the x and y dependencies of the self-field.) The result is the following expression for the self-field,

$$E_{s\pm}(x,y,z) = -\frac{1}{2}\frac{4\pi}{c}\int dx'\, H_T(x - x') \int dy'\, e^{\pm iky'}\, J_x(x',y',z) \ . \qquad (23)$$

Thus, the effective self-field at a point $\mathbf{x}$ is determined by smoothing the current distribution over a range of x' values. The smoothing is determined by the weighting function,

$$H_T(x - x') = \int_{-1}^{1} \frac{kdn_x}{2\pi} (1 - n_x^2)^{1/2}\, e^{ikn_x(x-x')} \ . \qquad (24)$$

The weighting function, H_T, has unit area and a width equal to one wavelength.

To carry out the smoothing procedure within the context of the present formulation, we consider the current density variable, J_x, appearing in Eqs. (6) - (18) to be the smoothed version of a local current J_μ

$$J_x(x,y,z) = \int dx'\, h\,(x - x')\, J_\mu\,(x',y,z) \ . \qquad (25)$$

The smoothed current density, J_x, produces an electric field, E_x, via Eq. (8), and the corresponding radiated power can be calculated from the product of J_x and E_x. If the local current J_μ is the respose to an electric field E_μ then we require that the power described by the product $J_\mu E_\mu$ be equal to that given by the product $J_x E_x$. This can be accomplished by choosing the electric field E_μ to be a smoothed version of the field E_x,

$$E_{\mu\pm}(x,y,z) = \int dx'\ h\ (x - x')\ E_{\pm}\ (x',y,z)\ . \tag{26}$$

Here, the smoothing function h is assumed to be a real, even function of its argument. Under these definitions, the rate of power transfer for the smoothed and unsmoothed quantities is the same,

$$\begin{aligned} P_D &= -\frac{1}{8}\int d^3x \left(J_x^* (E_+ e^{iky} + E_- e^{-iky}) + c.c.\right) \\ &= -\frac{1}{8}\int d^3x \left(J_\mu^* (E_{\mu+}\ e^{iky} + E_{\mu-}\ e^{-iky}) + c.c.\right)\ . \end{aligned} \tag{27}$$

That is, if the unsmoothed current J_μ is the response to the smoothed electric field $E_{\mu\pm}$, the rate of work done on this current is the same as that done by the unsmoothed field $E_\pm$ on the smoothed current J_x. In tern, due to the properties of paraxial equations, this rate of work also equals the power radiated.

It now remains to determine an appropriate form of the smoothing function, h. To do this, we will pick h so that the power radiated by a given local current matches, in a way to be discussed, the expression (20), when Eq. (23) is used to determine the self-field. In Eqs. (20) and (23), the current density variable should be understood to be the local current density J_μ. Making this replacement we arrive at a modified expression for the power radiated into free space,

$$P_R = \frac{\pi}{2c}\sum_{\pm k} \int dz dx dx'\ H_T\ (x - x')\ \left| \int dy\ j_\mu\ e^{-iky} \right|^2 \tag{28}$$

This same quantity can be obtained within the context of the paraxial approximation from Eq. (27) if we take Eq. (22) to determine the unsmoothed electric field for a given smoothed current density, and then

express the power radiated in terms of the unsmoothed current j_μ. The result is identical to Eq. (28) provided one makes the replacement

$$H_T(x - x') = \int dx'' \, h(x - x'') \, h(x'' - x') \, . \tag{29}$$

Thus, using the property that the Fourier transform of a convolution is the product of the Fourier transforms of the convolved terms we have

$$h(x - x') = \int_{-1}^{1} \frac{k dn_x}{2\pi} (1 - n_x^2)^{1/4} \exp\left(ikn_x (x - x'')\right) \, . \tag{30}$$

Due to the ad hoc nature of the smoothing process, we will represent h(x - x') as a Gaussian with a width equal to a wave length instead of numerically evaluating the transcendental function defined in Eq. (30),

$$h(x) \cong \frac{k}{\sqrt{8}} \exp\left(-\pi \frac{k^2 x^2}{8}\right). \tag{31}$$

This choice preserves the properties,

$$\int dx \; H_T(x) = 1$$

$$H_T(0) = \frac{k}{4}$$

implied by Eq. (29). The result is that the correct value of the power radiated is obtained in the limiting cases of a smooth current distribution or a rod like current distribution.

C. Representation of fields

Having introduced the smoothing procedure we now describe the particular coordinate representation for the fields in this resonator. The scattering object will have a cylindrical geometry whose axis is parallel to the z axis, and thus transverse to the axis of the cavity. Therefore, for efficient numerical solution of the governing equations, we will find it necessary to transform back and forth between systems of polar coordinates aligned parallel to the y and z axes. For example, the fields are most naturally represented and manipulated in a system of polar coordinates (r, θ, y) where

$$r = (x^2 + z^2)^{1/2} \tag{32a}$$

and

$$\tan\theta = \frac{x}{z}. \tag{32b}$$

In this coordinate system the amplitudes of the forward and backward going waves can be represented in terms of a Fourier series expansion in the angular variable, θ,

$$E_{\pm}(\mathbf{x}_{\perp}, y) = \sum_{l} E_{\pm}(r, l, y)\, e^{il\theta}, \tag{33a}$$

with

$$E_{\pm}(r, l, y) = \int \frac{d\theta}{2\pi} e^{-il\theta}\, E_{\pm}(\mathbf{x}_{\perp}, y). \tag{33b}$$

Similarly, the increments of radiation growth ($\Delta E_{\pm}(\mathbf{x}_{\perp})$ can also be represented in a Fourier series,

$$\Delta E_{\pm}(\mathbf{x}_{\perp}) = \sum_{l} \Delta E_{\pm}(r, l)\, e^{il\theta} \tag{34a}$$

with

$$\Delta E_{\pm}(r, l) = \int \frac{d\theta}{2\pi} e^{-il\theta}\, \Delta E_{\pm}(\mathbf{x}_{\perp}). \tag{34b}$$

With this representation the integral equations relating the fields on opposing mirrors separate into a system of one dimensional integral equations. For example, Eq. (17) becomes

$$E_+(r,\ l,\ d_r) = \int_{Lm} 2\pi r'dr'\ K_l(r,\ r',\ \sigma_t)\ E_+\ (r',\ l,\ -d_l)$$
$$+ \int 2\pi r'dr\ K_l(r,\ r',\ \sigma_r)\ \Delta E_+\ (r',\ l)\ , \tag{35}$$

where the Kernels can be expressed in terms of ordinary Bessel functions of order l,

$$K_l(r,\ r',\ \sigma) = \frac{-\ i\ e^{-il\pi/2}}{2\pi|\sigma|}\ J_l\left(\frac{rr'}{|\sigma|}\right) \exp\left(i\frac{(r^2 + r'^2)}{2|\sigma|}\right) \tag{36}$$

The boundary conditions, Eq. (10), also separate when fields are expressed in this polar coordinate system.

Our procedure for numerical solution of the governing equations will be the following. The fields in the resonator will be represented in polar coordinates with a Fourier decomposition in polar angle as in Eqs. (33) and (34). The currents in the scatterer are most easily calculated in a polar coordinate system aligned parallel to the z axis. Thus, the fields at the scatterer need to be transformed from their cavity axis polar representation to the Cartesian representation (as in (33a) and (34a)) and then smoothed. Once the fields at the scatterer are known, the currents in the scatterer can be calculated and smoothed. From these the change in field amplitude given by Eq. (12) can be evaluated first in Cartesian coordinates and then transformed to the cavity axis system as in Eq. (34b).

The solution is made self-consistent by iterating the above described procedure many times. We begin with a guess for the amplitude of the

waves leaving each of the mirrors and the amplitude of the self-field. The current in the scatterer, which is the response to these fields, is then calculated. This gives a new value for the self-field and allows one to determine the amplitudes of the fields incident on the mirrors. The procedure is then iterated until a steady state solution is achieved. During this iteration process, the value of the wave number k must also be updated in order to determine the frequency of oscillation of the mode. In addition, various convergence factors are introduced to realize a numerically stable algorithm.

In the next two sections, we will give examples of numerical solution of the governing equations for the cases in which the scatterer is 1) a thin dielectric annulus and 2) a gyrotron beam.

III. EFFECT OF A DIELECTRIC SCATTERER

The first series of calculations that we have performed were to determine the effect of an annular dielectric tube on the modes of a quasi-optical cavity. This problem was chosen since the results of the calculation could be compared with those of a relatively simple experiment.

The current density inside the dielectric material is linearly related to the local field intensity and the dielectric susceptibility of the material,

$$\frac{4\pi}{c} j_\mu = - ik(\varepsilon - 1) E_{\mu x} . \qquad (37)$$

where $E_{\mu x}$ is the local field within the dielectric tube. For a relatively weak dielectric ($|\varepsilon-1| << 1$) tube the fields inside and outside the dielectric are essentially the same. For a strong dielectric, $|\varepsilon-1| \geq 1$, the field inside the tube is shielded to some degree. If the tube is a thin annulus, the shielding can be estimated by assuming the field outside is predominately polarized in

the x direction and equating the tangential and normal components of the electric field and the electric displacement vectors respectively. Letting x and y be the coordinates of a point on true annulus of radius r_b we have

$$\frac{4\pi}{c} j_\mu = - ik(\varepsilon-1) \left(\frac{x^2 + \varepsilon y^2}{\varepsilon r_b^2} \right) E_{x\mu}$$

where $E_{x\mu}$ is now the field just outside the dielectric.

In the calculation, the scatter is broken into a large number, N, (typically 60) of small rods and the current in each rod is proportional to the cross-sectional area of the scatterer.

$$j_\mu = \frac{1}{N} \sum_{i=1}^{N} I_i(z)\ \delta(x - x_i)\ \delta(y - y_i) \qquad (38)$$

where

$$I_i(z) = - i \frac{kcA(\varepsilon - 1)}{4\pi} \left(\frac{x_i^2 + \varepsilon y_i^2}{\varepsilon r_b^2} \right) E_{\mu x}\ (x_i, y_i, z)\ . \qquad (39)$$

Here, x_i and y_i are the location of the i^{th} rod, and A the cross-sectional area of the scatterer.

The system of equations described in the previous section along with the constitutive relation Eqs. (38) and (39) was then solved to determine the complex eigenfrequency of a cavity with parameters relevant to experiments carried out at the CRPP. The parameters of the mirrors defining the cavity are given in Table 1. Here both mirrors are taken to be spherical, the left one being perfectly reflecting and the right one partially transmitting ($|\rho_r| = 0.95$, corresponding to a power transmission coefficient of 10%). In the experiment the right mirror was in fact a grating[12,13] with radius of curvature equivalent to that of Table 1. The phase of ρ_r was chosen so that resonant frequency of the cavity without the dielectric tube agreed with the simulation.

Figure 1 shows the effective cavity transmission coefficient

$$T_{eff} = 1 - \exp\left(\frac{-2\gamma d}{c}\right) \tag{40}$$

where γ is the temporal damping rate of the mode, as a function of the strength of the scatterer. Here the strength of the scatterer is measured by the parameter

$$I = \frac{16A(\varepsilon - 1)}{r_0\lambda} \tag{41}$$

where r_0 is the nominal spot size at the center of the cavity and λ the wavelength.

Figure 1 shows the effective transmission coefficient for the lowest order transverse mode with a frequency near 92.4 GHz for annular scatterers with two different radii and varying strength. As can be seen, the effective transmission coefficient is 0.10 when the scattering strength goes to zero. This transmission results almost entirely from the partial reflectivity of the right mirror. Due to the large size of the two mirrors, virtually no power spills around the mirrors in the absence of the scatterer. As the scattering strength is increased, scattered radiation spills over the sides of the mirror increasing the damping rate of the mode and consequently the transmission coefficient. Also shown on this plot are experimentally determined values of the transmission coefficient. The method by which these numbers were obtained will now be described.

To bench mark the code the quality factor of a Fabry-Pérot Resonator was measured at low power. The resonator consisted of a spherical mirror and a diffraction grating mounted in a -1 order Littrow arrangement.[13] Its two way loss T (T = 10%) is determined by the groove depth and the diffraction angle θ (θ = 28°). The other parameters of the resonator are:

g-factor = -0.71, separation between the grating and the mirror = 40 cm, mirror and grating size = 10 cm, nominal spot size r_0 = 0.93 cm. The coupling of microwave power into the resonator was performed by launching a gaussian beam with the correct waist on the grating. A fraction, 10%, of the power was thus transferred to the resonator. The quality factor Q and the implied two way loss T were determined from the resonance curve obtained by changing the microwave frequency in the vicinity of 92.4 GHz.

To simulate the electron beam, cylindrical tubes of Teflon (length = 10 cm >> spot size, wall thickness = 0.5 mm) were placed across the axis of the cavity. The location of the tube could be moved along the resonator axis. Tubes with different outer diameters (2.1 mm to 3.74 mm) were used to produce different degrees of scattering. Figure 1 presents the variation of the two way loss T versus the scattering strength I. The simulations and experiments were not performed for exactly the same parameters. In particular, in the simulation the mean radius of the tube is held fixed (two are shown, r_b = 1 mm and 2 mm) whereas in the experiment it varies. Furthermore, uncertainties in the absolute location of the dielectric tube will cause variations in the measured transmission coefficient due to the standing wave nature of the electric field in the cavity.

These discrepancies are eliminated by plotting the two way transmission coefficient versus displacement of the tube along the axis of the cavity for a given set of tube parameters. Such plots appear in Fig. 2. Figure 2(a) shows the case of a 2.18 mm diameter tube, while Fig. 2(b) shows the case of a 2.80 mm diameter tube. The solid points in Fig. 2(a) correspond to the measured transmissions and the open points correspond to the measured values shifted by 0.6 mm so as to match the simulated values which are given by the solid line. As can be seen the shifted experimental values and the simulated values agree quite well. The

experimental uncertainty in the absolute location of the tube is 0.5 mm, which is comparable to the value of the shift required to bring agreement. The agreement in the case of the 2.8 mm tube is less perfect. Here the experimentally measured transmission is somewhat less than the simulated value. This may be due to the experimental difficulty in aligning the larger tube across the axis of the resonator. Misplacement or tilting of the tube could yield a supplementary averaging of the strength of the incident electric field and hence a weaker interaction.

Figure 3 shows the magnitude of the simulated and the measured (and shifted) frequency shift as a function of the tube displacement for the 2.18 mm tube. The frequency shift is negative as the dielectric tube lowers the resonant frequency of the cavity. The simulated frequency shift is somewhat larger than that which is measured. However, the variation in frequency shift with displacement for the two cases is in good agreement.

Taking the preceding results to be an indication that the code is accurately simulating the field structure, we will now turn to the simulation of a resonator driven by an electron beam.

IV. SELF-CONSISTENT FIELD STRUCTURE WITH A GYROTRON BEAM

The second series of calculations we have performed were to determine the self consistent field structure in the cavity in the presence of a gyrating electron beam. The motivation for this study was to determine whether the scattering of radiation by the beam into large angles could degrade the efficiency with which the energy of the beam is extracted. Our basic conclusion is that for current and planned experiments the degradation of the efficiency with which power is collected is not large.

As in the case of a dielectric scattered, we modeled the beam as a number (typically 60) of current rods. This leads to an expression for the

current density which is identical to that given by Eq. (38). The individual rod currents, $I_j(z)$, are then determined by integrating the nonlinear, gyro-averaged equations of motion for an ensemble of weakly relativistic electrons in the presence of the calculated electric field. The calculation is then repeated iteratively until the electric field distribution comes to a steady equilibrium which is consistent with the calculated current. This then represents a nonlinear, saturated, single frequency state of the oscillator.

Figure 4 shows the results of one set of calculations in the form of plots of perpendicular efficiency versus detuning for a beam of 50 A in the cavity described Table 1. Here detuning is defined as the difference between the frequency of oscillation and the relativistic gyro-frequency of the electrons on injection, normalized to the time of flight through a distance equal to the nominal spot size.

$$\delta = (\omega - \Omega/\gamma_0) r_0/v_z \, .$$

In the above, $\Omega = |qB/mc|$ is the nonrelativistic cyclotron frequency with B the applied magnetic field and q and m are the charge and mass of an electron respectively, and v_z is the axial velocity, which in the weakly relativistic is assumed to be constant. The ratio $\alpha = v_\perp/v_z$ is chosen equal to 0.95.

The perpendicular efficiency is defined with respect to the energy in transverse motion of the injected electrons.

$$\eta_\perp = \frac{v_\perp^2(z=-\infty) - v_\perp^2(z=\infty)}{v_\perp^2(z=-\infty)} \, .$$

Two efficiencies are shown in the plot. The larger of the two corresponds to the efficiency with which energy is extracted from the beam. The smaller efficiency corresponds to the efficiency with which power is coupled out of the cavity, through the partially transmitting mirror. In computing this efficiency, only the power leaving the cavity in azimuthal symmetric fields is included.

For the detuning which optimizes efficiency about 46% of the available beam energy is converted to radiation, while about 40% of the beam energy is coupled through the mirror in azimuthally symmetric fields. According to Eq. (5) one would expect the difference between these two efficiencies to be about 3%. However, upon closer examination of the simulation results, the difference between these two efficiencies is not due primarily to scattered radiation which does not intersect the mirrors. Rather, it is due to the excitation of low order non symmetric modes in the cavity. This is illustrated in Fig. 5 where the magnitude of the field on the surface of the right mirror for the forward propagating wave is plotted. As can be seen, there is a large component of field with an azimuthal mode number, $l = 6$.

The cause of the excitation of these non symmetric modes can be traced to two effects. First, the mirror sizes are large compared with the nominal spot size. Thus, low order non symmetric modes have essentially the same quality factor as the desired symmetric mode. Losses are determined primarily by the partially transmitting mirror for these modes. Second, the resonator parameters that have been chosen lead to a near degeneracy in the resonant frequencies of the lowest order symmetric and certain non symmetric modes. This is seen by considering the formula for the resonant frequency of various modes in an ideal resonator,

$$\omega_{plm} = \frac{\pi c}{d}\left(p + \frac{l + m + 1}{\pi} \arccos g\right),$$

where p, l, and m are the axial, azimuthal, and radial mode numbers and $g = 1 - R_c/d$. For the chosen parameters, the value of g is -0.71 and consequently $\arccos g/\pi = 0.751$. Thus, a lowest order symmetric mode with indices ($p = p_0$, $l = 0$, $m = 0$) has nearly the same resonant frequency as a mode with ($p = p_0 - 6$, $l = 6$, $m = 2$). Other combinations are possible as well. The problem is that the factor $\arccos g/\pi$ is too close to the rational number, 3/4.

To illustrate how the excitation of these unwanted modes can be avoided we simulated a resonator with a separation d = 24.236 cm and a radius of curvature R_c = 17.78 cm. This leads to a value of the factor $\arccos g/\pi = 0.618$ which is the reciprocal of the golden mean $(1+\sqrt{5})/2$. The resulting field pattern, displayed in Fig. 6, shows markedly less excitation of non symmetric modes, and virtually all the power extracted from the beam is coupled out of the cavity in symmetric fields. In this case it seems that Eq. (5) overestimates the scattered radiation. The probable cause of the overestimation is the fact that the beam in the simulation is annular, with a size on the order of a wavelength, as opposed to being a pencil beam which is assumed in arriving at the back of the envelope calculation (5).

CONCLUSIONS

A numerical code has been developed to calculate the self consistent field structure in the open resonator of a quasi optical gyrotron. The results of the code compare favorably with experimental measurement of the quality factor and frequency of a resonator in which a dielectric tube is inserted. When the code is used to simulate the nonlinear state of a gyrotron oscillator it is found that the radiation from the electron beam can be well matched to the lowest order gaussian mode of the resonator provided

parameters are chosen with some care. In particular, it is advisable to avoid combinations of mirror spacing and radius of curvature for which there is a degeneracy between various low order transverse modes of an ideal cavity. This is particularly important if the resonator mirrors are large and power is coupled out of the cavity through a partially transmitting mirror. Finally, it is not likely that the observed, poorer than expected efficiency, in present experiments is due to excitation of nonsymmetric fields.

ACKNOWLEDGMENTS

This work was partly supported by the Fonds National Suisse de la Recherche Scientifique and the U. S. Department of Energy.

REFERENCES

1 P. Sprangle, J.L. Vomvoridis, and W. Manheimer, Phys. Rev. A **23**, 3127 (1981).

2 A. Bondeson, W.M. Manheimer, and E. Ott, Infrared & Millimeter Waves **9**, K.J. Button Ed., New York, Academic, 310 - 340 (1983).

3 S. Alberti, M.Q. Tran, J.P. Hogge, T.M. Tran, A. Bondeson, P. Muggli, A. Perenoud, B. Jödicke, and H.G. Mathews, Phys. Fluids **B2**, 1654 (1990).

4 A.W. Fliflet, T.A. Hargreaves, R.P. Fisher, W.M. Manheimer, and P. Sprangle, Journal of Fusion Energy, **9**, 31 (1990).

5 A.V. Gaponov et al., Int. J. Electron. **51**, 277 (1982).

6 K.E. Kreischer, R.J. Temkin, Phys. Rev. Lett. **59**, 547 (1987).

7 S.Y. Cai, T.M. Antonsen Jr., G. Saraph, and B. Levush, Int. J. Electron. **72**, 759 (1992).

8 W.C. Guss, M.A. Basten, K.E. Kreischer, R.J. Temkin, T.M. Antonsen Jr., S. Y. Cai, G. Saraph, and B. Levush, Phys. Rev. Lett. **69**, 3727 (1992).

9 A. Bondeson, and T.M. Antonsen Jr., Int. J. Electron. **61**, 855 (1986).

10 R.G. Kleva, T.M. Antonsen Jr., and B. Levush, Phys. Fluids **31**, 375 (1988).

11 J.D. Jackson, "Classical Electrodynamics", John Wily & Sons, New York (1975), Chapter 9.

12 J.P. Hogge, H. Cao, W. Kasparek, T.M. Tran, and M.Q. Tran, Fifteenth International Conference on Infrared and Millimeter Waves, R.J. Temkin, Editor SPIE, **1514**, 535 (1990).

13 M.Q. Tran, J.P. Hogge, H. Cao, W. Kasparek and T.M. Tran, J. Appl. Phys. **73**, 2089 (1993).

FIGURE CAPTIONS

FIG. 1. Effective transmission coefficient versus scattering strength for two dielectric tubes of radius 1 mm and 2 mm. Also shown are experimentally determined values for several dielectric tubes.

FIG. 2. Effective transmission coefficient versus displacement of the dielectric tube along the axis of the cavity for two tubes of diameter a) 2.18 mm and b) 2.80 mm.

FIG. 3. Magnitude of the frequency shift as a function of tube displacement for a tube of diameter 2.18 mm.

FIG. 4. Simulated efficiency versus detuning for an 50 A, 70 kV electron beam with beam velocity pitch ratio $v_\perp/v_z = 0.95$ and a 3 mm radius in the resonator whose parameters are listed in Table 1.

FIG. 5. Field magnitude on the output mirror in arbitrary units for the simulation of Fig. 4 with $\delta = 3.0$. The corresponding incident power density is about 1 MW/cm^2.

FIG. 6. Field magnitude on the output mirror in arbitrary units for the same conditions as Fig. 5 except the radius of curvature and mirror separation have been modified. The corresponding incident power density is about 2 MW/cm^2.

TABLE 1

Resonator Parameters :

Mirror Separation	=	40.0 cm
Mirror Radii of Curvature	=	23.5 cm
Mirror Radii	=	5.0 cm
Right Mirror Transmission	=	0.1
Nominal Spot Size	=	0.93 cm

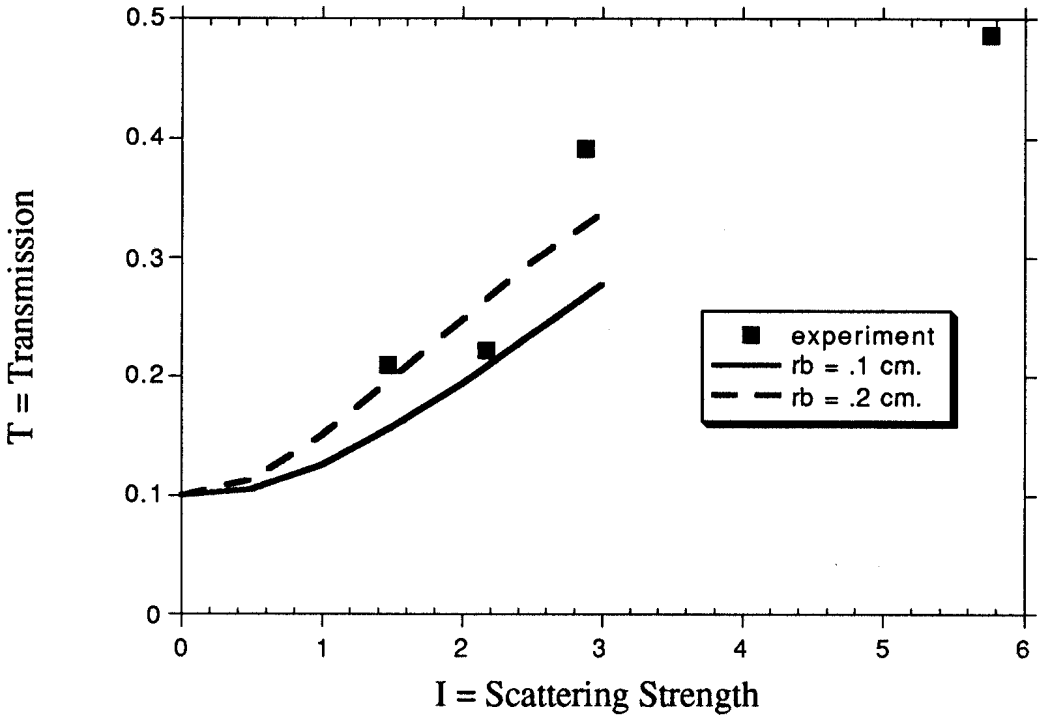
0.5
0.4
0.3
0.2
0.1
0
T = Transmission
0
1
2
3
4
5
6
I = Scattering Strength
experiment
rb = .1 cm.
rb = .2 cm.

Fig. 1

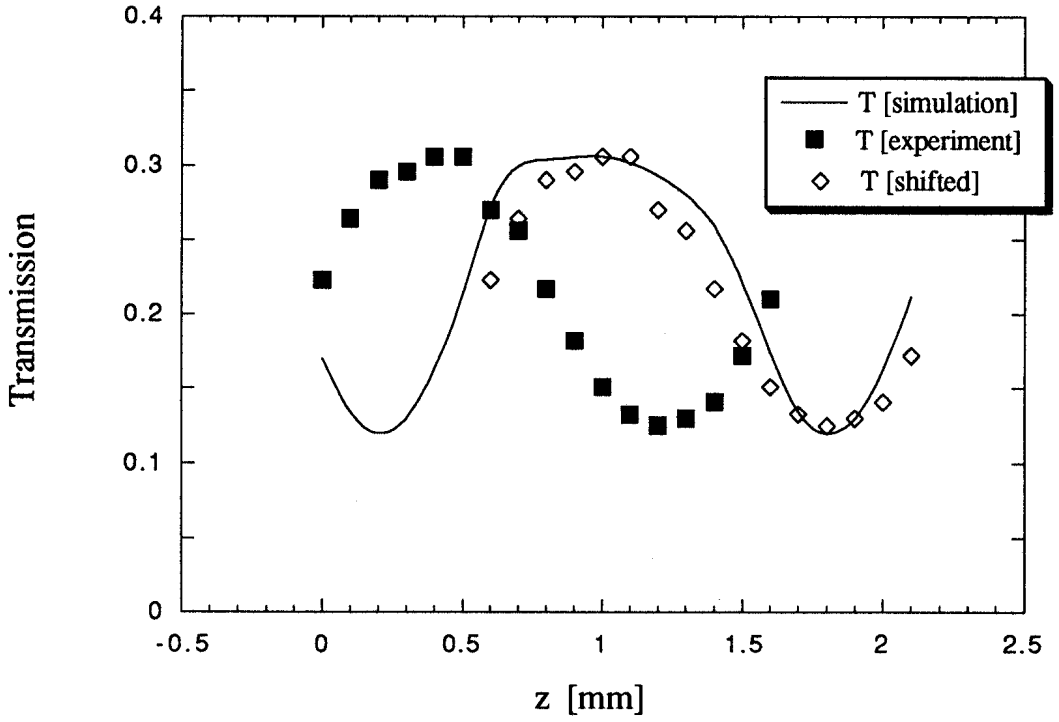
Transmission
0.4
0.3
0.2
0.1
0
-0.5
0
0.5
1
1.5
2
2.5
z [mm]
T [simulation]
T [experiment]
T [shifted]

Fig. 2a

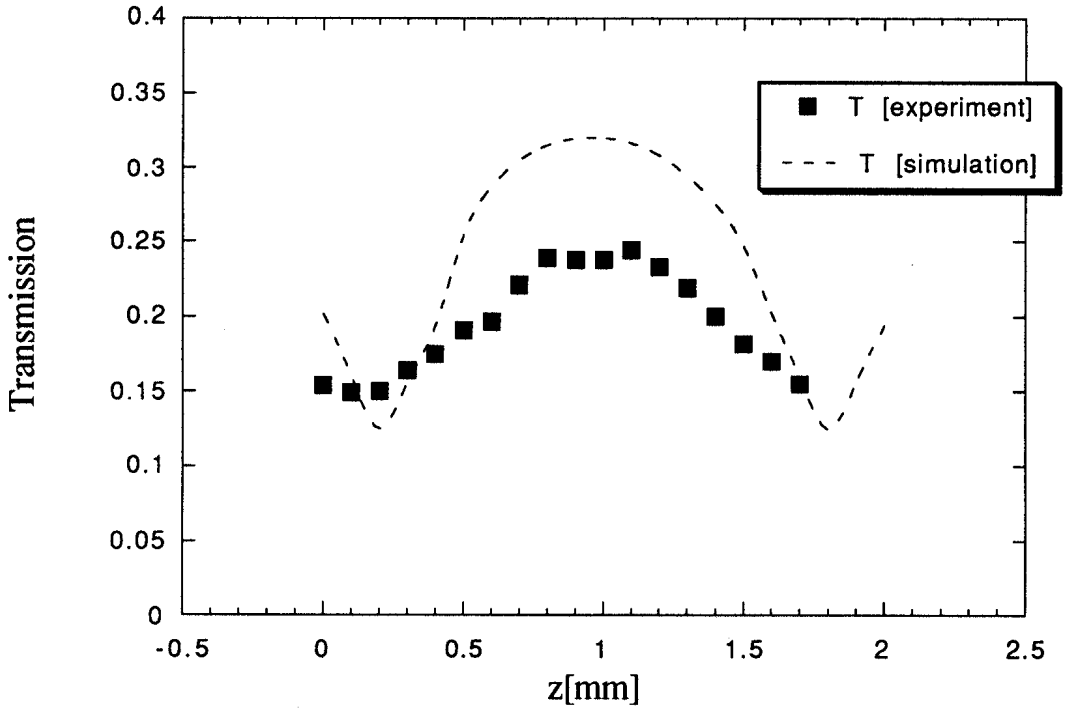
Transmission
0.4
0.35
0.3
0.25
0.2
0.15
0.1
0.05
0
-0.5
0
0.5
1
1.5
2
2.5
z[mm]
T [experiment]
T [simulation]

Fig. 2b

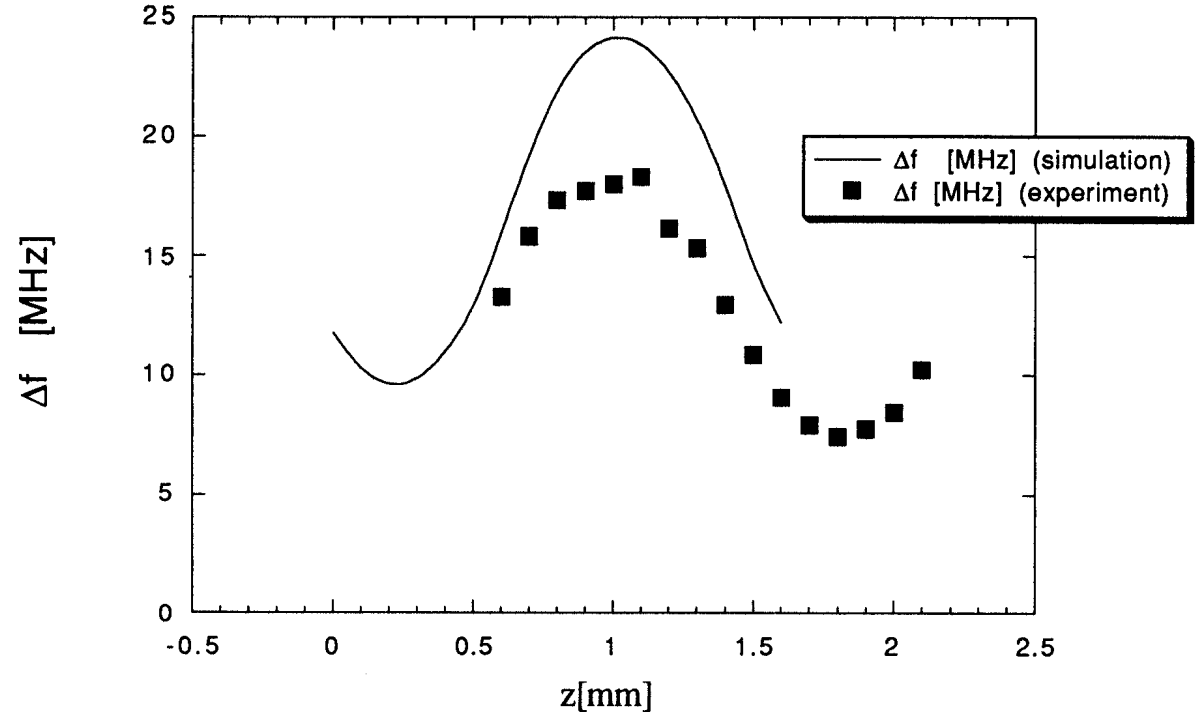
Δf [MHz]
25
20
15
10
5
0
-0.5
0
0.5
1
1.5
2
2.5
z[mm]
Δf [MHz] (simulation)
Δf [MHz] (experiment)

Fig. 3

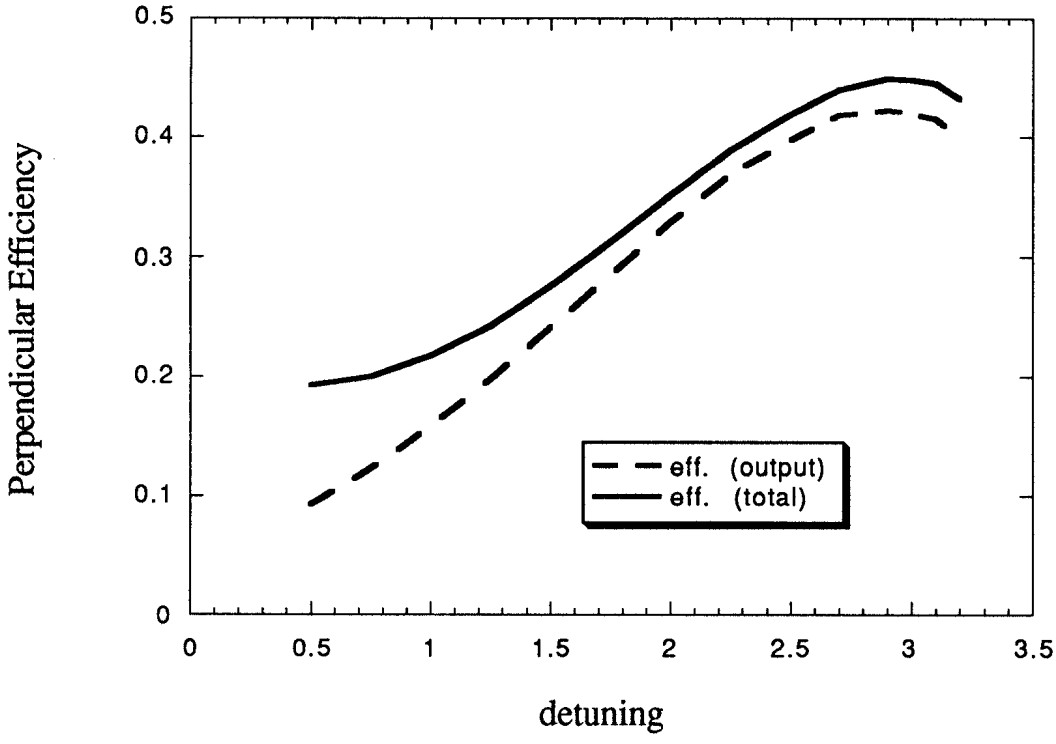
Perpendicular Efficiency
0.5
0.4
0.3
0.2
0.1
0
0
0.5
1
1.5
2
2.5
3
3.5
detuning
eff. (output)
eff. (total)

Fig. 4

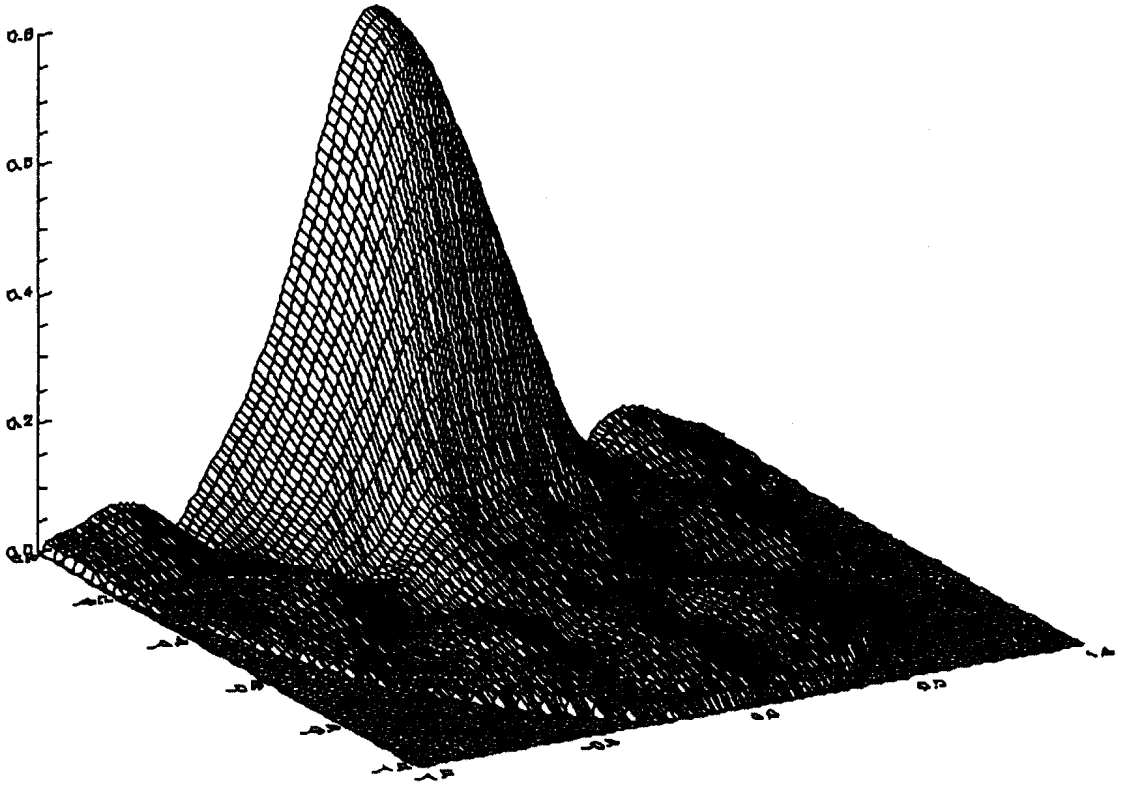

Fig. 5

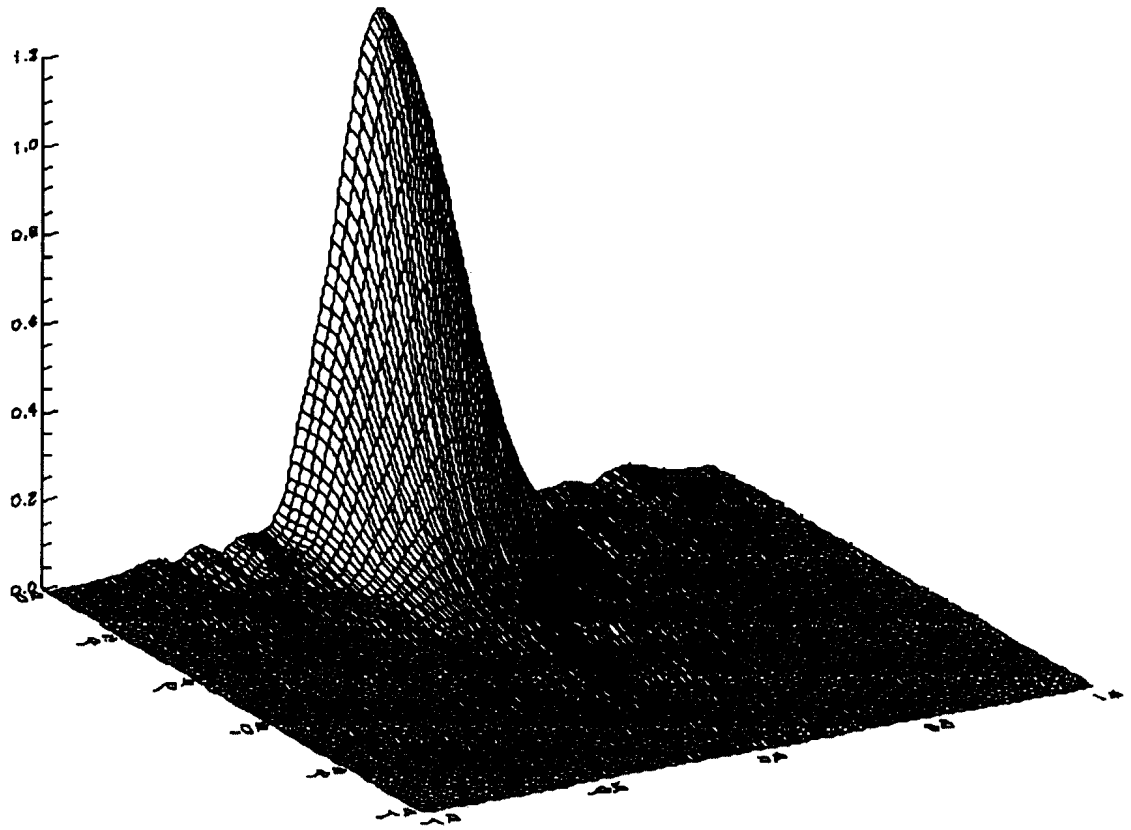

Fig. 6